European Journal of Pharmaceutics and Biopharmaceutics xxx (2014) xxx–xxx

Contents lists available at ScienceDirect

European Journal of Pharmaceutics and Biopharmaceutics

journal homepage: www.elsevier.com/locate/ejpb

Research paper

Structural attributes of model protein formulations prepared by rapid freeze-drying cycles in a microscale heating stage

Björn-Hendrik Peters *, Ferdinand Molnár, Jarkko Ketolainen

University of Eastern Finland, School of Pharmacy, Kuopio, Finland

ARTICLE INFO

Article history:
Received 20 November 2013
Accepted in revised form 27 February 2014
Available online xxxx

Keywords:
Freeze-drying
Microscale
Morphology
Micro-X-ray computed tomography
Scanning electron microscopy
Microcollapse
Lysozyme

ABSTRACT

Downscaled freeze-drying was demonstrated to be a valuable alternative for formulation development and optimization. Although the pore structure is known to exert a major influence on the freeze-drying cycle, little is known about the ones of microscale preparations. This study describes morphology evaluation methods for lysozyme formulations prepared in one microscale processing option and the assessment of fundamental product quality criteria. Scanning electron microscopy (SEM) revealed cooling rate dependent pore size variations at the nucleation site which diminished as the rate increased. Micro-X-ray computed tomography (μ-CT) showed that porosity generally increased in the sample from bottom to top, the pore size fractions shifted toward larger pores in elevated sample levels, and horizontal homogeneity was found throughout each sample with minor deviations in the bottom region. Furthermore, the event of microcollapse could be identified and quantified. Low residual moisture was achieved repeatedly and the procedure did not influence the post freeze-drying bioactivity. This microscale heating stage is a valuable option to reduce overall cycle times and cost, and to prepare freeze-drying formulations with high reproducibility. The mapping tools permit a quick but detailed insight into the structural features resulting from the process environment and processing conditions.

1. Introduction

Freeze-drying, also known as lyophilization, is a widely used process for handling biopharmaceuticals to ensure the maintenance of product stability and quality criteria during shipment and storage [1]. Designing a suitable product often entails a trial and error approach requiring substantial quantities of active pharmaceutical ingredient (API) and time to prepare candidate formulations. In this respect, trial and error are both expensive and inefficient. Adopting a rational formulation design based on scientific knowledge or utilizing external expertise could be a better approach but still involves a considerable number of choices as found from published recommendations [2,3]. Instead, reducing the needed amount of API by downscaling and simultaneously increasing the development efficiency by adopting a design of experiment (DoE) approach have been claimed as beneficial [4,5]. Nonetheless, the processing periods remain in the range of 15+ hours and as a result, the bottleneck of overall process cycle time must be addressed. In return the best candidate formulation may be quickly identified or formulation problems can be dealt with immediately. Even though in some cases adequate quantities of API are available, process duration remains a major delay factor. Freeze-drying cycle acceleration is often associated with optimization of the primary drying phase since one can shorten this phase by 13% per 1 °C elevated drying temperature [6]. This represents a significant increase in efficiency especially at the scaled up production levels. Be that as it may, the individual process optimization of each candidate formulation would not be resource efficient. Several studies have described outsourcing and shortening of the freezing step by directly placing formulation containers into varying cooling agents [7–9]. Unfortunately, freezing in a cooling bath differs drastically from shelf freezing and the morphological features, which are known to influence the sublimation rate [10], may well change in this situation. It is further important to appreciate the morphological design space of the process equipment,

Abbreviations: 2D, two-dimensional; 3D, three-dimensional; API, active pharmaceutical ingredient; DoE, design of experiment; DSC, differential scanning calorimetry; FDA, Food and Drug Administration; FDM, freeze-drying microscope/microscopy; Fr. I., fragmentation index; KF, Karl Fischer titration; K_v, heat transfer coefficient; NDCD, National Drug Code Directory; RGB, red–green–blue; RH, relative humidity; ROI, region of interest; R_p, resistance to vapor flow; SEM, scanning electron microscopy; T_c, collapse temperature; T_n, nucleation temperature; μ-CT, micro-X-ray computed tomography.

* Corresponding author. University of Eastern Finland, School of Pharmacy, P.O. Box 1627, Yliopistonranta 1C, FI-70211 Kuopio, Finland. Tel.: +358 50 594 455 3.
E-mail address: bjorn.peters@uef.fi (B.-H. Peters).

http://dx.doi.org/10.1016/j.ejpb.2014.02.016
0939-6411/

meaning here the relation of cycle input parameters and the resulting lyophilized cake morphology. Micro-X-ray computed tomography (μ-CT) can be valuable in this respect: it has a major benefit of not applying force to the fragile cake structure, thus being a non-destructive technique [11]. One common factor in all of the above described approaches is that they facilitate laboratory scale or pilot scale freeze-dryers and do not utilize a microscale freeze-drying cell. In 1994, a basic model of the current freeze-drying microscope (FDM) heating stage was introduced to provide a convenient means of direct observation of freezing and freeze-drying processes [12]. The FDM is regularly used to assess a formulation's collapse temperature (T_c), a critical process factor in freeze-drying cycle optimization. The T_c is arguably superior to the glass transition temperature of the maximal concentrated solution which is determined by differential scanning calorimetry (DSC) [13]. In addition, it should be noted that the T_c depends on the total solid content, the formulation, and weakly the nucleation temperature (T_n) and is best described as a range in which collapse occurs [14]. This knowledge has also practical implications e.g. for freeze-drying performed at the edge of the T_c. Here the phenomenon of microcollapse, leading to increased porosity, permitted higher vapor flow rates and thus a significant reduction of the primary drying time was achieved while the macroscopically elegant cake structure was maintained [15]. The cycle optimization described in Ref. [15] was also performed at pilot scale, limiting its usefulness for application in early developmental stages. Subsequently, there have been significant improvements made to the equipment e.g. utilizing silver as primary heating element material to provide high thermal conductivity, a prerequisite for efficient heat transfer, and addition of a liquid nitrogen pump to enlarge the operational temperature range. With regard to the temperature controlled shelf of tray freeze-dryers, the microscale heating stage yields the potential to be a realistic scaled down version: the silver heating element replaces the tray and liquid nitrogen replaces the cooling fluid. This study describes a time saving approach for microscale freeze-drying utilizing a FDM heating stage. The morphology of the dried cakes was studied by scanning electron microscopy (SEM) and μ-CT to provide insights into the formation of pores. In order to evaluate the potential for rapid biopharmaceutical formulation development, a model protein with biological activity was examined. Sucrose and trehalose were chosen as lyoprotectants both representing the most commonly used disaccharides [16]. Furthermore, mannitol was identified as the most frequent additive according to the freeze-drying formulations listed in the National Drug Code Directory (NDCD) from 1992 to 2012 published by the Food and Drug Administration (FDA). The residual moisture content, a critical factor with respect to protein stability, was introduced as a secondary end point and assessed by coulometric Karl Fischer titration (KF).

2. Materials and methods

2.1. Materials and formulations

Hen-Egg White Lysozyme was obtained from Dalian Greensnow Egg Products Development Co., Ltd. (Jinggang Industrial Area, Dalian City, China). Mannitol, sucrose, trehalose dihydrate, naproxen and methanol were purchased from Sigma Aldrich (St. Louis, MO, USA). Water was produced immediately before use by filtration in a Milli-Q-Gradient station equipped with a Millipak Express 0.22 μm filter (EMD Millipore, Billerica, MA, USA). The model formulations and their corresponding drying temperatures and processing times are summarized in Table 1.

2.2. Freeze-drying equipment

Freeze-drying was performed with a THMS350V heating stage (Linkam Scientific Instruments Ltd., Guildford, Surrey, UK). The heating stage was supplemented with a liquid nitrogen pump LNP94/2, a temperature controller TMS 94 (both Linkam Scientific), a vacuum pump E2M1.5 and a Pirani gauge (both Edwards Group Ltd., Crawley, West Sussex, UK). The equipment was controlled via the Linksys32 (Linkam Scientific) software package. The silver heating element's thermocouple was calibrated as described before [14] with the addition of water and naproxen for melting points of 0.0 °C and 156.1 °C, respectively. The melting point of naproxen was determined with DSC 823e (Mettler Toledo, Columbus, OH, USA).

2.3. Freeze-drying process – SEM samples

About 5 μl of silicon oil was spread between the silver heating block and a cover glass #1 with a diameter of 15 mm (Menzel GmbH, Braunschweig, Germany) to ensure close contact. The sample height was set by a 70 μm aluminum spacer (Biopharma Technology Ltd., Winchester, Hampshire, UK). A sample droplet volume of 0.3 μl and the surrounding spacer were placed directly onto the cover glass followed by a second cover glass on top. Each formulation was frozen at cooling rates of 5 °C, 10 °C and 20 °C/min down to −50 °C and held for 8 min with pressure reduction to 50 mTorr (approximately 6.67 Pa) starting after 4 min of holding time. The drying temperature was approached at a heating rate of 5 °C/min. Drying temperatures for all formulations described in Table 1 have been defined by applying a safety regimen of approximately

Table 1
Freeze-drying protocols for SEM (0.3 μl) and μ-CT, KF and bioactivity (200 μl) assessment.

	Target drying temperature (°C)[a]	Drying time (min)	Total processing time (min)[b]
Mannitol (1.10% w/V) + Lysozyme (2.00% w/V)			
SEM	−23	15	57.5; 61; 68
μ-CT, KF, bioactivity	−23	40	111.4
Sucrose (2.08% w/V) + Lysozyme (2.00% w/V)			
SEM	−28	20	62.5; 66; 73
μCT, KF, bioactivity	−28	75	146.4
Trehalose (2.08% w/V) + Lysozyme (2.00% w/V)			
SEM	−24	15	57.5; 61; 68
μ-CT, KF, bioactivity	−24	75	146.4

All samples were frozen down to −50 °C and held for 8 min. Cooling rates (°C/min) were 10 for μ-CT, KF, and bioactivity, and 5, 10, and 20 for SEM samples. The pressure during the freeze-drying process was held at 50 mTorr.

[a] The target drying temperature was determined in a preliminary T_c assessment by FDM and the introduction of a 5 °C safety range.

[b] The total processing time includes the beginning of the freezing process until the release of the sample from the heating stage.

Please cite this article in press as: B.-H. Peters et al., Structural attributes of model protein formulations prepared by rapid freeze-drying cycles in a microscale heating stage, Eur. J. Pharm. Biopharm. (2014), http://dx.doi.org/10.1016/j.ejpb.2014.02.016

5 °C to the average collapse onset determined in triplicate. The drying times were determined empirically by microscopic observation of the sublimation front during preliminary studies. After completion of the drying step, the silver block was heated at 5 °C/min to 30 °C for 15 min.

2.4. Freeze-drying process – μ-CT, KF and bioactivity samples

The sample volume was increased to 200 μl and the sample shape was made cylindrical as preferred for μ-CT imaging (Fig. 1). An in-house manufactured, hollow and circular shaped polypropylene sample holder was utilized. In addition, the cooling rate was fixed at 10 °C/min and the heating protocol following the drying step was changed to a 2 °C/min gradual increase with two holdings of 5 min after every 4 °C and two holdings of equal length after every 5 °C temperature increase. Drying times were accommodated to the higher sample volume. The remaining features of the heating procedure were as described for the SEM samples.

2.5. Scanning electron microscopy

All samples had the upper cover glass removed and were coated with gold for 60 s at 20 mA utilizing an auto sputter coater type B7341 (Agar Scientific Elektron Technology UK Ltd., Stansted, Essex, UK) to prevent sample charging. The cover glass carrying the coated sample was then placed directly inside the sample chamber of a XL30 ESEM (Fei Company, Hillsboro, OR, USA) for imaging at an acceleration voltage of 15 kV and a working distance of 12–15 mm. SEM images were obtained from 0.3 μl samples of all formulations. These represent the portion of the 200 μl samples in closest contact with the heating stage and therefore, the area in which nucleation would occur.

2.6. Micro-X-ray computed tomography

The μ-CT assessment was performed with a Skyscan 1172 (Bruker MicroCT, Kontich, Belgium) with medium camera settings and the microfocused X-ray source set to 35 kV (211 mA). Images were acquired every 0.25° for a full rotation of 360° at a voxel resolution of 4.5 × 4.5 × 4.5 μm. The sample placement was performed by direct release from the cylindrical sample holder onto a μ-CT sample holder equipped with double sided tape to prevent the lyophilized cake from moving during the rotation steps. The influence of moisture uptake was greatly reduced due to the dry climate conditions in the North-Eastern region of Finland during winter and the rapid handling of the specimen. Daily weather recordings of the Kuopio Airport (approximately 17 km from the experimental location) during the period when measurements were done reveal a temperature range of −24 °C to +3 °C with the relative humidity (RH) being between 25.2% and 100% (The Norwegian Meteorological Institute, Oslo, Norway). The reconstruction into three-dimensional (3D) cross-sections was conducted using the NRecon software package (Bruker MicroCT). In the subsequent image processing, the CTAn software package (Bruker MicroCT) was utilized and the analytic performance was adopted from an earlier description by Parker et al. [11]. The grayscale indices applied for separation of pores from the solid in the binary image were 0–9 for mannitol and trehalose, and 0–12 for the sucrose containing formulations with the remaining values up to 255 describing the solid sample part. The indices were set with air as the reference and confirmed by comparison of the binary with the original reconstructed grayscale image at the highest magnification. In the subsequent assessment, a set of 500 binary images was created from each sample, starting from the closest decade superior to the first fragment free grayscale image. The 500 images related to a cylindrical area of 2258.58 μm in height and 7453.32 μm in diameter ensured the coverage of the major part and an identical volume of each evaluated freeze-dried cake. The CTAn calculation results, directly used for reporting included the two-dimensional (2D) and 3D porosity, structure separation, and the fragmentation index (Fr. I.). In brief, the 2D porosity was calculated per individual cross-sectional plane as a percentage of the area enclosed by a solid against the total sample area of the binary image. Similarly, the 3D porosity calculated by the CTAn software was the result of a volume comparison of the solid and porous sample parts as defined by the binary image. Model-independent volumes were estimated by a volume-based local thickness fitting method applying maximal spheres to all points in the structure [17]. Subsequently, the individual points of neighboring spheres were subjected to a sphere inclusion test [17] meaning that each point is finally included in only one sphere. The volume was then given by summing the single spheres' volume with a stochastic error corresponding to the resolution [17], being 4.5 μm here. Structure separation, the method utilized to assess the pore size distribution within the sample, also used the local thickness fitting technique, but referred the spheres to the pore space. The resulting sphere diameters reflect the pore size distribution. The Fr. I. represents a connectivity index based on convexity and concavity [18]. The calculation method utilized the change in the trabecular surface and volume at image dilation resulting in lower values for connected structures [18]. The use of Fr. I. is recommended to be limited to relative comparisons.

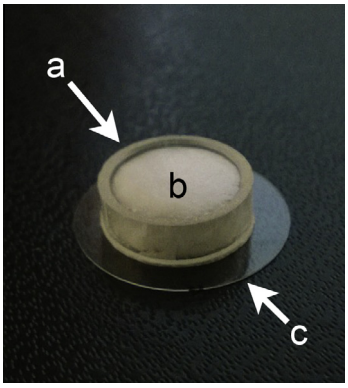

Fig. 1. Photograph of a 200 μl sample displaying the polypropylene sample holder (a), the freeze-dried cake (b) and the bottom cover glass (c). (For interpretation of the references to color in this figure legend, the reader is referred to the web version of this article.)

2.7. MATLAB® data analysis

Data analysis was performed with MATLAB® version 7.12.0.635 R2011a (The MathWorks, Natick, MA, USA) on the data sets based on the identical binary images used in the CTAn calculations. The first method was devised to calculate the overall porosity of a RGB (red–green–blue) image. Therefore, the region of interest (ROI) was cut from the binary image and placed against a colored background. Image separation was performed with Adobe Photoshop® CS5 Extended Version 12.0.3 × 32 (Adobe Systems, San Jose, CA, USA) without any alterations to the blending options. The porosity of the ROI was then determined by a counting method calculating the black fraction of the total black and white region. This method was used to evaluate porosity variations between the inner and outer sample region at a specific sample height but it can be generally applied to any user determined ROI. The second method was created to permit a quick visual inspection of sample variations at a specific sample height as determined by the chosen binary image. Here the image was divided into cells consisting of 25 × 25 pixels. The porosity of each cell was calculated as a

Please cite this article in press as: B.-H. Peters et al., Structural attributes of model protein formulations prepared by rapid freeze-drying cycles in a microscale heating stage, Eur. J. Pharm. Biopharm. (2014), http://dx.doi.org/10.1016/j.ejpb.2014.02.016

percentage of black against total pixels. High porosity fragments at the sample edge resulting from a cell including a majority of black image background pixels were filtered by introducing a rule of altering edge cells of porosity greater than 50% to the background color. The edge localization verification was implemented as a function of linear indexing for neighbor comparison.

2.8. Residual moisture content

The residual moisture content was measured with a C30 Compact Karl Fischer Coulometer (Mettler Toledo, Columbus, OH, USA). The freeze-dried sample was reconstituted with 1 ml of dry methanol and homogenized. A volume of 900 µl was then pipetted into the KF cell. Based on the original reconstitution volume and the water content of an equal volume of dry methanol the sample water content was calculated.

2.9. Fluorescence-based lysozyme activity measurements

The activity of the lysozyme in the samples was measured using EnzChek Lysozyme Assay Kit (Invitrogen E-22013) according to the recommendation of the manufacturer. Briefly, the freeze-dried samples were resuspended in 1 ml Milli-Q water and then consequently diluted to a concentration 0.4 µg/ml of lysozyme. To 25 µl of the diluted sample, the same amount of 1X reaction buffer – component B (100 mM sodium phosphate pH 7.5, 100 mM NaCl, 2 mM sodium azide as a preservative) was added in the white 96-well ViewPlate (PerkinElmer 6005181). Subsequently 50 µl of a 50 µg/ml working suspension of the fluorescent DQ lysozyme substrate was added to the mixture and the samples were incubated for 30 min at 37 °C in the dark. The fluorescence intensity of each reaction was measured in an EnVision 2004 multilabel reader equipped with monochromators set to excitation at 494 nm and emission at 518 nm.

3. Results

3.1. Scanning electron microscopy

An elegant macroscopic sample appearance was achieved without exception although cracks within the cake structure could be detected under magnification. The incidence of these cracks was found to begin with the meeting of the sublimation fronts at the sample center. SEM images of a formulation consisting of mannitol 1.10% w/V and lysozyme 2.00% w/V at the different cooling rates of 5 °C/min, 10 °C/min and 20 °C/min from top to bottom are shown in Fig. 2. The general structural features of the sample preparation setup reveal a smooth cake layer adjacent to the cover glass interrupted only by the cracks as described previously. The qualitative difference in pore size between the edge regions presented on the left against the center regions depicted on the right is seen for cooling rates of 5 °C/min and 10 °C/min of the mannitol formulation while it diminishes at a higher cooling rate. The pore size difference for sucrose and trehalose formulations was found to be generally less pronounced (images not shown). As an approximation for the mannitol samples, surface pore sizes are found below 3 µm for a cooling rate of 5 °C/min at the sample edge (A.1) and up to 5 µm at the sample center (A.2). The majority of surface pores at cooling rates of 10 °C/min and 20 °C/min at the sample edge appear to be below 2 µm (B.1, C.1). The sample center at the cooling rate of 10 °C/min (B.2) shows pores of up to 3 µm while at 20 °C/min (C.2) there is no longer any difference compared to the sample edge (C.1) in qualitative terms. Given the limitations of the SEM for evaluating the actual 3D pore proportions, these values are only indicative. Nonetheless, the variations of pore size in the smooth surface layer are very limited. In particular, the edge region's appearance remains to be independent of the applied cooling rates. As crack occurrence allows a view of sample parts that is not in contact with the glass cover lid (assumed from image A.2 and B.2) both the pore diameter and porosity increase rapidly as the distance increases from the cover glass.

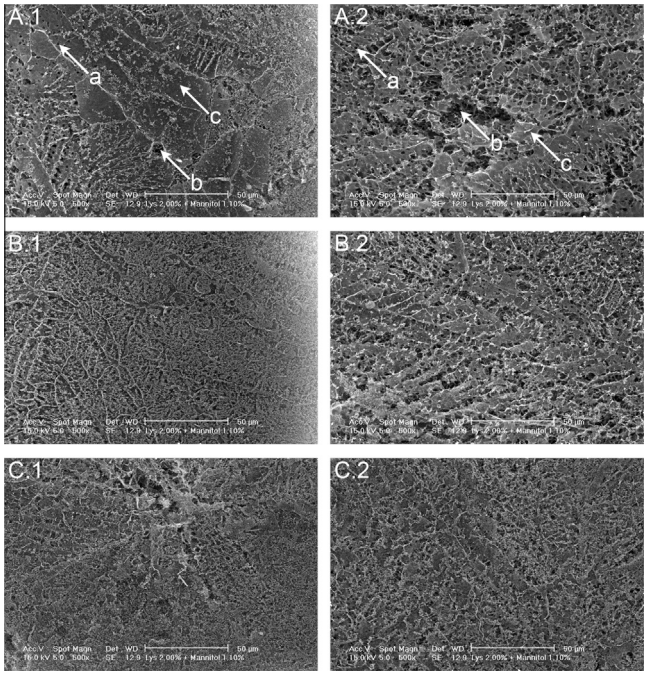

Fig. 2. All samples for imaging are prepared from 0.3 µl of a 1.10% w/V Mannitol + 2.00% w/V Lysozyme formulation as described in Table 1. SEM images on the left display the sample edge region while those on the right show the center region. The cooling rate (°C/min) was 5, 10 and 20 for the images A.1 + A.2, B.1 + B.2, and C.1 + C.2, respectively. The arrows indicate surface pores (a), cracks (b), and dry matter (c).

3.2. Micro-X-ray computed tomography

In order to understand the 3D structural characteristics and to supplement the SEM observations, the analytical method of µ-CT was employed to evaluate five samples of each formulation. All samples had an elegant macroscopic appearance. The T_n of each sample was recorded immediately at the moment at which nucleation was visually observed. Furthermore, it was noted that nucleation occurred at the sample bottom in direct proximity to the heating stage with subsequent freezing directed toward the sample surface.

3.2.1. 3D evaluation of complete samples

The observed T_n, the sample porosity, and the Fr. I. are given in Table 2. Independent of the T_n, the total porosity reflects a freeze-drying process with reproducible structural features. In addition, this finding is supported by the negative Fr. I. found in all five samples for each formulation revealing also the highly interconnected structures. While the Fr. I. values for all mannitol and sucrose formulations are situated in a narrow range, the value of −0.086 obtained for trehalose + lysozyme sample 3 reveals a greater deviation from the other samples prepared from the same formulation, reflecting a less comprehensively interconnected structure in relative terms. The pore size distribution is given in Fig. 3 for all formulations with the spherical diameter of the pores as descriptor. Irrespective of the excipient used in the formulations, the distribution remained similar. The smallest pores (4.52–13.55 µm) represent 16.70% (±0.97), 17.44% (±0.73), and 18.27% (±2.00) of the full

Please cite this article in press as: B.-H. Peters et al., Structural attributes of model protein formulations prepared by rapid freeze-drying cycles in a microscale heating stage, Eur. J. Pharm. Biopharm. (2014), http://dx.doi.org/10.1016/j.ejpb.2014.02.016

Table 2
Nucleation temperature, 3D-porosity, and Fr. I. of freeze-dried cakes.

Sample	T_n (°C)	Porosity (%)	Fr. I.
Mannitol (1.10% w/V) + Lysozyme (2.00% w/V)			
1	−12.9	50.35	−0.095
2	−10.1	50.72	−0.088
3	−11.9	50.83	−0.090
4	−10.9	49.93	−0.097
5	−13.8	50.52	−0.087
Average		50.47 (±0.35)	−0.091 (±0.004)
Sucrose (2.08% w/V) + Lysozyme (2.00% w/V)			
1	−12.3	48.24	−0.096
2	−8.9	48.81	−0.090
3	−11.5	48.64	−0.096
4	−11.4	48.03	−0.103
5	−10.6	49.36	−0.093
Average		48.61 (±0.52)	−0.096 (±0.005)
Trehalose (2.08% w/V) + Lysozyme (2.00% w/V)			
1	−15.9	46.71	−0.114
2	−12.4	47.77	−0.103
3	−10.7	51.37	−0.086
4	−13.1	47.53	−0.112
5	−14.8	47.66	−0.102
Average		48.21 (±1.82)	−0.103 (±0.011)

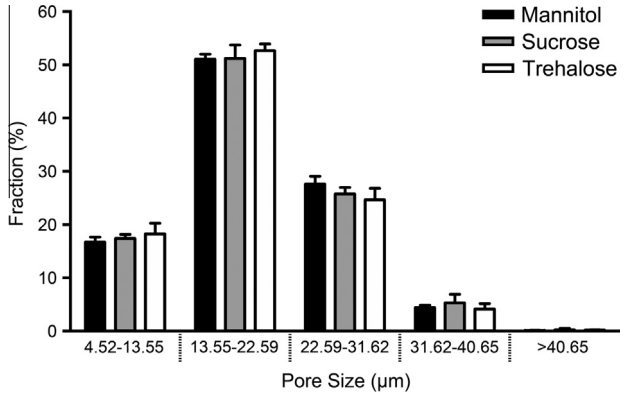

Fig. 3. Pore size distribution average of all five samples of each individual formulation. Black represents the mannitol, gray the sucrose, and white the trehalose formulations of lysozyme.

pore space for the mannitol, sucrose, and trehalose formulations, respectively. The majority was found in the region between 13.55–22.59 µm with fractions of 51.07% (±0.97), 51.20% (±2.53), and 52.65% (±1.25). The remaining pores are found mostly within the diameters of 22.59–40.65 µm with less than 1% of the pores being found in an even larger fraction. These findings suggest that this was a conservative freeze-drying cycle. With the application of a 5 °C safety regimen between the formulations' T_c and the drying target temperature as reported in Table 1, a conservative process cycle would comply with the process design's intention. However, the total average values of 3D calculations are able to mask the variation occurring within and between samples requiring a deeper analysis of the binary images and a separation of each dataset into its critical parts.

3.2.2. Sample homogeneity – a combined 2D/3D approach

The 2D porosity variation for all five samples of the mannitol, sucrose and trehalose formulations is illustrated from bottom to top in Fig. 4. The SEM result indicated that there was an increased porosity at increasing distances from the bottom, which is strictly found in case of all lysozyme preparations formulated in mannitol.

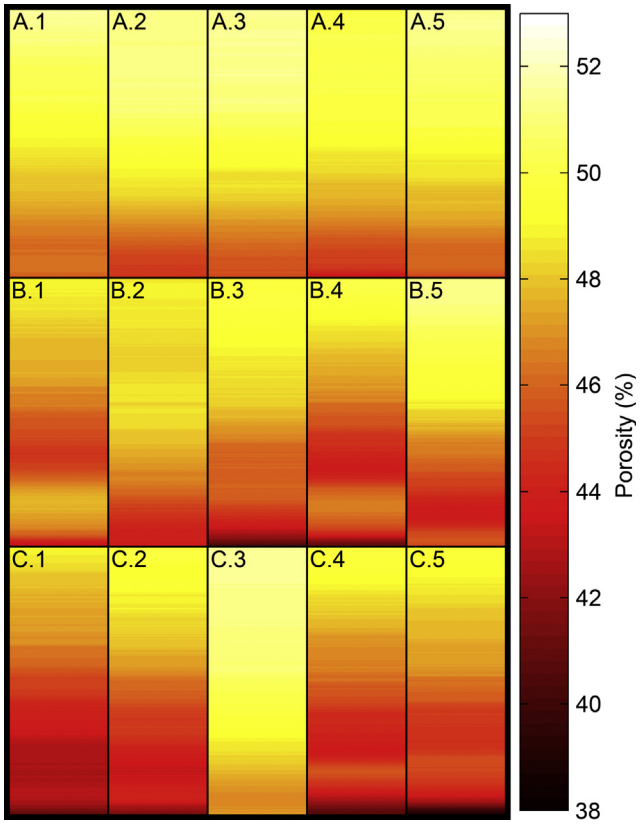

Fig. 4. Representation of 2D-porosity per individual dataset image. Each dataset consists of 500 reconstructed grayscale images obtained by µ-CT. A.1–A.5, B.1–B.5, and C.1–C.5 show results for lysozyme formulations in combination with mannitol, sucrose, and trehalose, respectively. Each section (e.g. "A.1") shows the porosity of the respective sample from bottom (lower section part) to top (upper section part). (For interpretation of the references to color in this figure legend, the reader is referred to the web version of this article.)

This general trend is equally applicable for the preparations of sucrose and trehalose formulations but individual sample areas deviate and show higher porosity than expected. This observation is thought to be an indication of microcollapse. Due to maintenance of an overall high connectivity at local shifts toward an increased pore size, this observation is not strongly reflected and easily identified in the Fr. I. The remaining variation found in the porosity pattern is explained by the random nature of the nucleation event and the deviation of the nucleation temperature which cannot be controlled by the heating stage. Special attention needs to be paid to the trehalose + lysozyme sample 3 denoted as "C.3" which clearly displays a higher porosity than other samples with the same composition. In fact, only continual increasing porosity toward the sample surface was seen. Just as for the Fr. I. proposed by Parker et al. [11] as indicator of microcollapse, this would also suggest that the vertical 2D variation is not a sufficient indicator.

3.2.3. Microcollapse determination

In order to link the observed variations to pore size distribution and finally to decide whether microcollapse had actually occurred, each dataset was further divided into four subsets of 125 binary images. Two characteristic examples are shown in Fig. 5. The top and bottom part of mannitol sample 1 denoted as mannitol 1.1 and mannitol 1.4, respectively, is shown in Fig. 5A. The pore size fractions in both subsets are shown as deviations from the average pore size distribution in the total dataset. It was found that the pore size fraction with the diameter between 4.52 and 22.59 µm was significantly higher at the bottom of the sample with a shift

Please cite this article in press as: B.-H. Peters et al., Structural attributes of model protein formulations prepared by rapid freeze-drying cycles in a microscale heating stage, Eur. J. Pharm. Biopharm. (2014), http://dx.doi.org/10.1016/j.ejpb.2014.02.016

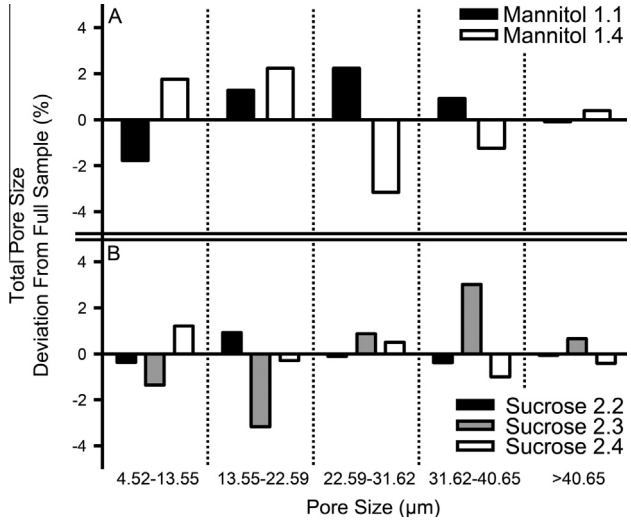

Fig. 5. Total percentage deviation of the pore size fractions within regions of interest (125 images each) denoted as *.1 to *.4 (top to bottom) from the complete dataset (500 images). (A) Mannitol sample 1 represents a conservative freeze-drying process based on directed solidification without microcollapse. (B) Sucrose sample 2 represents the event of microcollapse in region of interest 3 exhibiting a decrease in small pore and an increase in large pore fractions compared to adjacent regions.

toward an increased pore size fraction of 22.59–40.65 µm at the top of the sample. Furthermore, a slightly higher than average fraction of pores larger than 40.65 µm was found in the bottom part of the sample. This finding contradicted with the general trend and it is thought to be related to the cracks appearing at process cycle completion as earlier described. Fig. 5B represents the bottom and the next two higher subsets of sucrose sample 2 denoted as sucrose 2.4, 2.3, and 2.2. The sudden decrease of the pore size fraction in the range from 4.52 to 22.59 µm was accompanied by a 5.45% increase in the fraction larger than 22.59 µm for sample parts 2.4–2.3, respectively. The fact that this trend discontinued in sample subset 2.2 was indicative of a postfreezing pore size distribution change, i.e. microcollapse. When one considers the trehalose + lysozyme sample 3, no sudden decrease in the smallest fraction 4.52–13.55 µm was seen, instead there was a constant decrease as the sample height increased. On the other hand in the fraction 13.55–22.59 µm, a decrease from 51.87% to 48.96% was encountered between the bottom and adjacent upper subset. This decrease was accompanied by an increase for the fraction 31.62–40.65 µm from 3.15% to 7.18% and discontinued in the proximate upper subset, revealing an event of microcollapse. In addition to the localization of microcollapse events, the appearance of this distinction from the full dataset pore size distribution makes it possible to conduct a ROI related quantification. A complete list of pore size distributions for all subsets can be found in the Supplementary data. Furthermore, a full picture of the structural features requires a description of horizontal homogeneity in conjunction with the results depicting vertical variations. A straightforward differentiation between critical areas is obtained by the segmentation of the binary image into an inner and outer region with the distance between the center point and the regions' common border being equal to the distance between the border and sample edge. Table 3 shows the variation of each sample, created by the calculation of the difference in the porosity for five adjacent binary images located at the bottom, center, and top of the dataset. Irrespective of the excipient, a significant deviation ranging from 3.75% (±0.04) to 11.24% (±0.15), 2.95% (±0.07) to 13.65% (±0.23), and 5.27% (±0.43) to 7.82% (±0.29) was observed between the inner and outer sample region at the bottom of the freeze-dried cake for mannitol, sucrose, and trehalose formulations, respectively.

Table 3
Comparison of center and edge 2D-porosity of freeze-dried cakes.

Sample	Porosity (%)		
	Bottom	Center	Top
Mannitol (1.10% w/V) + Lysozyme (2.00% w/V)			
1	11.24 (±0.15)	1.86 (±0.06)	1.00 (±0.06)
2	3.87 (±0.15)	0.88 (±0.03)	1.08 (±0.05)
3	3.75 (±0.04)	0.69 (±0.10)	0.95 (±0.03)
4	6.89 (±0.12)	1.66 (±0.06)	1.53 (±0.10)
5	10.44 (±0.09)	1.33 (±0.06)	1.53 (±0.11)
Sucrose (2.08% w/V) + Lysozyme (2.00% w/V)			
1	9.54 (±0.44)	1.01 (±0.09)	1.51 (±0.04)
2	2.95 (±0.07)	1.92 (±0.02)	1.67 (±0.03)
3	5.72 (±0.07)	0.51 (±0.14)	0.55 (±0.31)
4	3.84 (±0.52)	0.69 (±0.24)	0.75 (±0.04)
5	13.65 (±0.23)	1.47 (±0.08)	1.12 (±0.05)
Trehalose (2.08% w/V) + Lysozyme (2.00% w/V)			
1	7.82 (±0.29)	1.36 (±0.12)	1.31 (±0.04)
2	6.67 (±0.13)	0.79 (±0.03)	1.58 (±0.11)
3	5.27 (±0.43)	1.87 (±0.10)	1.75 (±0.04)
4	6.75 (±0.07)	0.73 (±0.13)	1.10 (±0.05)
5	6.34 (±0.36)	1.47 (±0.19)	1.05 (±0.09)

The huge ranges in the bottom sample area are the consequence of the cracking which cannot be prevented. At an increasing sample height, the difference tends to disappear, with variations clearly below 2% for all formulations at the center and top levels. An attempt to address the potential oversight of the variations within the distinct areas, a complementary evaluation method which utilizes visual control of porosity changes by comparing the color scale of neighboring cells is described (Fig. 6). The bottom, center, and top binary images of the mannitol sample 1 are shown denoted as A.1, A.2, and A.3, respectively. Image A.1 displays a high porosity in the center of the sample which clearly deviates from the remaining area. The color bar indicates that the porosity is higher than 80% which is attributable to the formation of cracks in the bottom of the sample area. This observation of bottom cracks was made for all formulations. Images A.2 and A.3 show a rather consistent color pattern with a slight tendency toward increased porosity in the central part of image A.2 which disappears according to the visual inspection in image A.3 completely.

3.3. Bioactivity and residual moisture content

The freeze-dried samples were assessed within 2 h after completion of the third sample's freeze-drying cycle and were continuously stored on ice during that interval. Table 4 reveals the remaining bioactivity of each formulation ($n = 3$) as the relative percentage of the formulation's activity before freeze-drying and the residual moisture content ($n = 3$) as a volume percentage. No significant bioactivity loss was found with or without the presence of a stabilizing agent. The residual moisture content of each formulation was assessed directly after completion of each sample's freeze-drying cycle. The low residual moisture content was not found to have any impact on the bioactivity of lysozyme and this was reproducible and independent of which additive was used.

4. Discussion

4.1. Scanning electron microscopy

The investigation of 0.3 µl samples by SEM revealed only a marginal influence of the cooling rate on the pore size appearance independent of the used additive. The surface pore radii from the SEM images appear to be within the range of 1–2.5 µm which is comparable to the range of 2–20 µm described earlier by Pikal and Shah [19]. Fonseca et al. [20] reported that the T_c varied only

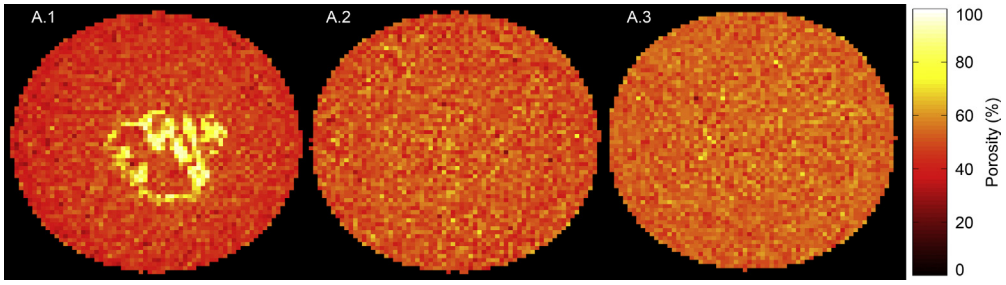

Fig. 6. Representation of the sample homogeneity by calculating the average porosity per 25 × 25 pixel array of mannitol formulation sample 1 (volume 200 µl, cooling rate 10 °C/min). The images A.1, A.2 and A.3 are calculated from the bottom, center, and top binary image of the full dataset, respectively. (For interpretation of the references to color in this figure legend, the reader is referred to the web version of this article.)

Table 4
Postfreeze-drying bioactivity and residual moisture content.

	Lysozyme (2.00% w/V) +			
	–	Mannitol (1.10% w/V)	Sucrose (2.08% w/V)	Trehalose (2.08% w/V)
Bioactivity (%)		105.64 (±4.35)	94.04 (±4.61)	94.30 (±0.93)
Residual moisture (% V/V)	–	0.12 (±0.03)	0.05 (±0.02)	0.12 (±0.02)

by 1 °C for a 5% w/w sucrose solution at cooling rates between 1 °C/min and 10 °C/min. The direct influence of structural features on key factors of the freeze-drying process such as sublimation rate and the final pore structure has been described by Hottot et al. [10]. The observations of the limited variation in ice crystal morphology at varying cooling rates support the finding of the limited T_c variation. The sample cracks described earlier were found after completion of the freeze-drying cycle. Therefore it is suggested, that they did not result from collapse or influenced the T_c assessment. Furthermore, these cracks did also not originate from microcollapse and thus did not promote a faster freeze-drying cycle.

4.2. Micro-X-ray computed tomography

3D µ-CT data indicate that the freeze-dried cake had been formed from a conservative freeze-drying cycle. The Fr. I. indicates a highly interconnected structure with the pore size mainly distributed between 4.52 and 40.65 µm. The existing smaller pores, which were found in the nucleation zone by SEM assessment, were not detectable with the given µ-CT resolution. From the visual observation of quickly increasing pore sizes at elevated SEM sample levels the authors assume that a limited pore fraction was excluded by the µ-CT assessment. This leads to a potential overestimation of the solid content as discussed by Stange et al. [21] for vial freeze-drying and a spatial resolution of 9 µm. In comparison with the corresponding values presented by Parker et al. [11] for a pilot scale process, the smaller pore size can be generally seen as a feature of the process and its environment. It seems to be a logical causality that the reduced sample volume limits the space available for ice crystal growth and the large sample bottom area in relation to the volume promotes heat exchange with the tray and thus quick freezing. The reader is referred to the "The Microscale Approach – A Comparison" section for a more detailed discussion of the pore size differences. Independent of the actual pore size, the available tools for assessing porosity variations in horizontal and vertical directions in combination with the calculation of porosity and pore size of ROIs provide a deeper insight into structural features than can be obtained with the overall 3D results. As expected for directed solidification, the average 2D porosity reveals a structural trend due to the continuous porosity increase toward the surface but identifies deviating areas as well. When combining the 2D vertical variation with horizontal grid separation, true structural changes can be distinguished from local sample defects. The subsequent definition of ROIs based on the sample dimensions and the observed variation can then be used in the quantification. A related finding is that the Fr. I. alone is not an adequate indicator of microcollapse. In our previous example for the sucrose formulations the Fr. I. value is comparable with the one of the other lysozyme + sucrose samples independent of the presence or absence of microcollapse. In contrast, for trehalose + lysozyme sample 3, which was clearly different from the other samples, the possible microcollapse was indicated by a strongly deviating Fr. I. However, microcollapse was found only to a minor extent while the overall structural characteristics of the sample appeared to have much greater influence on the Fr. I. Utilizing the vertical 2D porosity representation to determine ROIs in combination with both horizontal analysis methods to ensure the sample homogeneity, microcollapse can be demonstrated and quantified via a change in pore size distribution deviating from the general trend of increasing pore size in each upper vertical sample level. We consider this method as being superior to the approach based only on Fr. I. values. Nevertheless, it should be noted that knowledge about the solidification process is not a prerequisite for microcollapse detection, but is vital to formulation and process cycle development. With regard to visualization of the features reflecting the horizontal structure, grid cell size is a critical factor. A grid defined from large cells may mask significant local variations within a cell and cause visual detection errors. A 25 × 25 pixel grid where each cell represents approximately 0.03% of the total sample area was considered as an acceptable compromise for this study but we believe that decision has to be taken on a case by case basis. Furthermore, it should be noted that the constraints for the exclusion of edge artifacts resulting from image processing can lead up to 5.97% of the total sample area not being represented in the horizontal grid. However, this has only a limited effect on the visual observation of variations. Increasing the cell dimensions possibly increases also the area detected as part of an edge artifact and thus the final determination of the cell size must always be related to the total sample dimensions.

4.3. Solidification process

As already outlined, the determined structural features are in good agreement with the observed solidification process. All of

Please cite this article in press as: B.-H. Peters et al., Structural attributes of model protein formulations prepared by rapid freeze-drying cycles in a microscale heating stage, Eur. J. Pharm. Biopharm. (2014), http://dx.doi.org/10.1016/j.ejpb.2014.02.016

the examined samples followed the definition of directional solidification as introduced by Searles et al. [22]. This behavior is thought to be a result of the high heat conductivity of the silver heating block and the missing gap between this shelf and the thin cover glass posing a relatively small resistance to the heat transfer compared to the gas phase found between shelf and vial in larger scale freeze-drying processes [23,24]. The high heat conductivity in combination with the freezing rate of 10 °C/min subsequently leads to the vertical temperature gradient required for directional solidification. It must be mentioned that global supercooling was observed for the sucrose formulation with T_n between −15.5 °C and −16 °C (lowest T_n achieved) while no such phenomenon was noted for formulations with mannitol or trehalose. These findings indicate that directional solidification can be achieved when a vertical temperature gradient can be established inside the sample. Nonetheless, because of the random nature of the nucleation event, it appears that below a critical temperature, the impact of the vertical temperature gradient is reduced and the nucleation zone encompasses the full sample as described for global supercooling by Searles et al. [22]. Samples following this global supercooling pattern collapsed during the drying process. This is thought to be a result of the increased resistance to vapor flow (R_p) requiring a prolonged drying time, for which the process cycle was not designed. Importantly, the freeze-drying cell's ability to achieve directed solidification is a major advantage when aiming for reduced formulation development runtimes since higher drying rates can be achieved [22]. The completion of the freeze-drying cycle was achieved rapidly; the total processing time could be reduced by at least 83% in comparison with the holding times of the ultra scale down freeze-drying method presented previously by Grant et al. [4,5].

4.4. Bioactivity and residual moisture content

In terms of postfreeze-drying bioactivity, the experimental setup did not influence the properties of lysozyme. This finding is well in agreement with the results presented by Liao et al. [25]. They detected no bioactivity loss in formulations including sucrose or trehalose and 92.6% (±5.7) of the original activity without addition of a stabilizing agent. Furthermore no influence of residual moisture content on bioactivity was reported between 0.9% w/w and 8.3% w/w which is also in good agreement with our results [25]. No evidence was found for protein denaturation with the rapid cooling rates used in this study although this will need to be confirmed since the lysozyme concentrations were relatively high and the absence of denaturation may be due to self-stabilization [26].

4.5. The microscale approach – a comparison

While the sample volume of 200 µl is in good agreement with the range of 100–200 µl used earlier in well-plate approaches [4,5,27], differences to classic vial configurations must be discussed. Specifically heat flux, nucleation temperature, sample container, cooling rate, pore morphology, and scale up potential should be considered. The heat flux is proportional to the temperature difference between shelf and container bottom when including the heat transfer coefficient (K_v) as proportionality factor. The K_v is expected to differ in the contribution of the underlying components from vial freeze-drying as the gas filled gap between the shelf and the vial bottom is eliminated by the plane cover glass and silicon oil, creating a tight connection to the heating element. Reduced gas conduction and increased direct conduction from the heating element to the bottom glass, in relative terms, are fair speculation. Radiation, depending on the surface area, the emissivity, and the temperature of a given material, is also expected to contribute significantly, especially as the effect of Plexiglas doors is well-known [28,29]. Due to the use of the microscale heating stage for microscopic T_c assessment, a window centered above the sample is present in this setup as well. As a consequence of the achievable heat flux, directional solidification can be exploited, if required. Nevertheless, the critical attribute during the drying phase regarding final product quality and appearance is the product temperature [30]. The shelf temperature simply has to be adjusted accordingly to account for the changed heat fluxes. Furthermore, this microscale equipment's viable temperature range covers the one of manufacturing process cycles without exception.

The T_n of all 200 µl samples at a cooling rate of 10 °C/min (Table 2) is in good agreement with the T_n of vial freeze-drying configurations reported by multiple authors [10,31,32]. Still, methodological differences in T_n assessment must be taken into account. Every T_n reported in this paper refers to the shelf temperature at the moment of nucleation, Hottot et al. [10] fixed thermocouples outside the vial wall and the vial bottom, and both Kuu et al. [31] and Konstantinidis et al. [32] placed thermocouples inside the vial. With regard to the following comparisons it should also be mentioned that Nakagawa et al. [33] fixed thermocouples outside the vial wall at half the vial filling height. While not directly measuring the sample temperature, the benefit of an external temperature measurement is not to introduce additional nucleation spots known to result in an increased T_n [34].

The sample container, consisting of the cover glass and cylindrical polypropylene holder, resembles the vial bottom and sidewall and grants the sample a vial-configuration-like shape. Inter-vial variation of the sublimation rate depending on the shelf location of a respective vial [35] and variation resulting from inconsistent pre-stoppering depth are thought to be mostly excluded in this microscale approach due to the experimental setup.

The high cooling rate of 10 °C/min used for the 200 µl samples was initially utilized to further reduce the overall cycle time by shortening the freezing step. More common manufacturing cooling rates in the range of 1 °C/min can be achieved, if required. More interestingly, the presented morphological data are in good agreement with the effect of cooling rates on ice crystal mean sizes simulated by Nakagawa et al. [33]. The reported ice crystal mean size at a T_n range of −14 °C to −8 °C was approximately 20–24 µm for a 10% mannitol solution at a cooling rate of 5 °C/min, respectively [33]. Applying the calculation method to the µ-CT data sets revealed a pore mean size of 19.56–20.31 µm, 19.35–20.70 µm, and 18.90 µm to 20.23 µm for the respective lysozyme formulations of mannitol, sucrose, and trehalose at a cooling rate of 10 °C/min. Furthermore this indicates, that the pore mean size is independent of the formulation and a high cooling rate reduces the impact of the random nucleation event, thus, supports reproducibility. The simulated vertical variation of ice crystal mean size range was approximately 16–50 µm (T_n = −14 °C) and 20–70 µm (T_n = −8 °C) at a cooling rate of 1 °C/min [33]. Importantly, the simulated range appears quite close to the range of 2–40.65 µm observed for a cooling rate of 10 °C/min utilizing the microscale heating stage. A study by Hottot et al. [10] investigated the effects of vial types, filling heights, and freezing protocols on the ice crystal morphology of a 5% w/w BSA model formulation. While the cumulative distribution of ice crystal mean diameters showed the possibility of variations between different vial types, the reported mean ice crystal diameter range from approximately 20 µm to 160 µm was similar [10]. This range is significantly higher compared to the study of Nakagawa et al. [33] and this microscale approach, but in good agreement with the pore size range reported by Parker et al. [11] for an aggressive freeze-drying cycle utilizing microcollapse of a 0.5% w/V BSA and 2.5% w/V sucrose model formulation, which was 4.33–160.29 µm [11]. In addition, the mean ice crystal diameter assessed by optical microscopy was reported to be 70 µm [10] which

Please cite this article in press as: B.-H. Peters et al., Structural attributes of model protein formulations prepared by rapid freeze-drying cycles in a microscale heating stage, Eur. J. Pharm. Biopharm. (2014), http://dx.doi.org/10.1016/j.ejpb.2014.02.016

far exceeds the size expected by the model of Nakagawa et al. [33]. The increase of the ice crystal mean diameter at an increased filling height [10] is in agreement with the observation of the pore size distribution changing toward larger pore diameters at elevated sample heights. The conservative freeze-drying cycle of the aforementioned BSA + sucrose model formulation revealed a pore size distribution of 4.33–73.65 μm [11], being in good agreement with both, the simulation results [33] and our microscale approach. Conclusions should only be drawn carefully from these comparisons, as model formulations, nucleation procedures, freezing protocols, sample containers, filling heights, filling volumes, solid content and assessment methods vary. The authors therefore assume, that the microscale approach yields the potential to resemble the pore size range of scaled up equipment while the pore size distribution leans toward smaller pores, but this must be reviewed as further data become available.

Assessment of the scale up potential and transferability is currently highly speculative. From the impact of the vial and the freezing protocol on the ice crystal size distribution demonstrated by Hottot et al. [10] it is already indicated, that a transfer of the process must be performed for each vial type of interest, especially bearing the different heat transfer characteristics of polymer vials in mind [36]. On the other hand, the transfer of cycles utilizing K_v and R_p, which are based on the factors discussed above, has been demonstrated earlier [37]. Further obstacles are related to the formulation. Considering mannitol, high cooling rates could lead to a reduced crystallized amount of mannitol [38] and in return cause formulation instability at large scale equipment with a lower cooling rate when a larger fraction of mannitol crystallizes and becomes unavailable for hydrogen bonding. Also, when thinking of surfactants, the surface areas resulting from directional solidification and global supercooling could require different amounts to achieve the same level of API stabilization. On the other hand, speaking in relative terms for equal freezing mechanisms, the larger fraction of small ice crystals leads to an ice–water interface larger than in scaled up equipment. Stable microscale formulations of biopharmaceuticals prone to degradation at the ice–water interface [26] could thus be utilized immediately.

5. Conclusion

The presented data demonstrate the feasibility of the microscale heating stage to substantially reduce the time required for an individual freeze-drying cycle while resembling multiple attributes found in vial freeze-drying. The preservation of the post-freeze-drying bioactivity which is a prerequisite for a successful biopharmaceutical formulation development was achieved successfully on the model protein. The applied nature of this study is emphasized by the inclusion of three of the most relevant additives used in currently marketed lyophilized pharmaceuticals. The general reproducibility of freeze-dried samples was demonstrated by μ-CT while the developed mapping tools for visualization of structural features and the method of defining critical sample areas appear to represent a quick and logical approach to cake characterization. Furthermore an extended morphological design space of the processing environment is indicated by the potential to control the freezing mechanism. Utilizing lysozyme as a model protein this study should be seen as a starting point to establish this approach for rapid formulation development. Future investigations have to extend the applicability of this microscale approach to the processing of significant biopharmaceutical and biotechnological products, assess the effects of the cooling rate on formulation stability and transferability, and to examine the cycle transfer from microscale to scaled up processes.

Sources of support

FinPharma Doctoral Program (Funding of the position).
PROMIS Centre Consortium (Provision of equipment).
SIB Labs, the Department of Applied Physics, and the School of Pharmacy, all University of Eastern Finland (Technical support).
The funding sources had no involvement in study design, collection, analysis, and interpretation of the data, in the writing of the report, and in the decision to submit the article for publication.

Acknowledgments

The authors gratefully acknowledge the financial support of the FinPharma Doctoral Program and the provision of equipment by the PROMIS Centre consortium (supported by the Finnish Funding Agency for Technology and Innovation (Tekes), the Regional Council of Pohjois-Savo, the North Savo Centre for Economic Development, Transportation and Environment, and participating industrial partners). In addition the authors thank Dr. Arto Koistinen (SIB Labs, University of Eastern Finland), Mr. Markus Malo (Department of Applied Physics, University of Eastern Finland) and Ms. Viktória Prantner (School of Pharmacy, University of Eastern Finland) for the technical help with the μ-CT studies.

Appendix A. Supplementary material

Supplementary data associated with this article can be found, in the online version, at http://dx.doi.org/10.1016/j.ejpb.2014.02.016.

References

[1] M.J. Pikal, Freeze drying, in: J.S. Swarbrick, J.C. Boylan (Eds.), Encyclopedia of Pharmaceutical Technology, Marcel Dekker, New York, 2002, pp. 1299–1326.
[2] J. Carpenter, M.J. Pikal, B. Chang, T. Randolph, Rational design of stable lyophilized protein formulations: some practical advice, Pharm. Res. 14 (1997) 969–975.
[3] M.J. Pikal, Freeze-drying of proteins, Part II: Formulation selection, BioPharm 3 (1990) 26–30.
[4] Y. Grant, P. Matejtschuk, P. Dalby, Rapid optimization of protein freeze-drying formulations using ultra scale-down and factorial design of experiment in microplates, Biotechnol. Bioeng. 104 (2009) 957–964.
[5] Y. Grant, P. Matejtschuk, C. Bird, M. Wadhwa, P. Dalby, Freeze drying formulation using microscale and design of experiment approaches: a case study using granulocyte colony-stimulating factor, Biotechnol. Lett. 34 (2012) 641–648.
[6] M.J. Pikal, Freeze-drying of proteins, Part I: Process design, BioPharm 3 (1990) 18–27.
[7] J. Iwai, N. Ogawa, H. Nagase, T. Endo, T. Loftsson, H. Ueda, Effects of various cyclodextrins on the stability of freeze-dried lactate dehydrogenase, J. Pharm. Sci. 96 (2007) 3140–3143.
[8] T. Suzuki, K. Imamura, H. Fujimoto, M. Okazaki, Relation between thermal stabilizing effect of sucrose on LDH and sucrose-LDH hydrogen bond, J. Chem. Eng. Jpn. 31 (1998) 565–570.
[9] K. Tanaka, T. Takeda, K. Miyajima, Cryoprotective effect of saccharides on denaturation of catalase by freeze-drying, Chem. Pharm. Bull. 39 (1991) 1091–1094.
[10] A. Hottot, S. Vessot, J. Andrieu, Freeze drying of pharmaceuticals in vials: influence of freezing protocol and sample configuration on ice morphology and freeze-dried cake texture, Chem. Eng. Process.: Process Intensif. 46 (2007) 666–674.
[11] A. Parker, S. Rigby-Singleton, M. Perkins, D. Bates, D. Le Roux, C.J. Roberts, C. Madden-Smith, L. Lewis, D.L. Teagarden, R.E. Johnson, S.S. Ahmed, Determination of the influence of primary drying rates on the microscale structural attributes and physicochemical properties of protein containing lyophilized products, J. Pharm. Sci. 99 (2010) 4616–4629.
[12] S. Nail, L. Her, C.B. Proffitt, L. Nail, An improved microscope stage for direct observation of freezing and freeze drying, Pharm. Res. 11 (1994) 1098–1100.
[13] E. Meister, H. Gieseler, Freeze-dry microscopy of protein/sugar mixtures: drying behavior, interpretation of collapse temperatures and a comparison to corresponding glass transition data, J. Pharm. Sci. 98 (2009) 3072–3087.
[14] E. Meister, S. Sasic, H. Gieseler, Freeze-dry microscopy: impact of nucleation temperature and excipient concentration on collapse temperature data, AAPS PharmSciTech 10 (2009) 582–588.
[15] R.E. Johnson, M.E. Oldroyd, S.S. Ahmed, H. Gieseler, L.M. Lewis, Use of manometric temperature measurements (MTM) to characterize the freeze-

drying behavior of amorphous protein formulations, J. Pharm. Sci. 99 (2010) 2863–2873.
[16] W. Wang, Lyophilization and development of solid protein pharmaceuticals, Int. J. Pharm. 203 (2000) 1–60.
[17] T. Hildebrand, P. Rüegsegger, A new method for the model-independent assessment of thickness in three-dimensional images, J. Microsc. 185 (1997) 67–75.
[18] M. Hahn, M. Vogel, M. Pompesius-Kempa, G. Delling, Trabecular bone pattern factor—a new parameter for simple quantification of bone microarchitecture, Bone 13 (1992) 327–330.
[19] M.J. Pikal, S. Shah, The collapse temperature in freeze drying: dependence on measurement methodology and rate of water removal from the glassy phase, Int. J. Pharm. 62 (1990) 165–186.
[20] F. Fonseca, S. Passot, O. Cunin, M. Marin, Collapse temperature of freeze-dried *Lactobacillus bulgaricus* suspensions and protective media, Biotechnol. Prog. 20 (2004) 229–238.
[21] U. Stange, M. Scherf-Clavel, H. Gieseler, Application of gas pycnometry for the density measurement of freeze-dried products, J. Pharm. Sci. 102 (2013) 4087–4099.
[22] J.A. Searles, J.F. Carpenter, T.W. Randolph, The ice nucleation temperature determines the primary drying rate of lyophilization for samples frozen on a temperature-controlled shelf, J. Pharm. Sci. 90 (2001) 860–871.
[23] S.L. Nail, The effect of chamber pressure on heat transfer in the freeze drying of parenteral solutions, PDA J. Pharm. Sci. Technol. 34 (1980) 358–368.
[24] M.J. Pikal, M.L. Roy, S. Shah, Mass and heat transfer in vial freeze-drying of pharmaceuticals: role of the vial, J. Pharm. Sci. 73 (1984) 1224–1237.
[25] Y. Liao, M. Brown, A. Quader, G. Martin, Protective mechanism of stabilizing excipients against dehydration in the freeze-drying of proteins, Pharm. Res. 19 (2002) 1854–1861.
[26] B.S. Chang, B.S. Kendrick, J.F. Carpenter, Surface-induced denaturation of proteins during freezing and its inhibition by surfactants, J. Pharm. Sci. 85 (1996) 1325–1330.
[27] H. Trnka, J.X. Wu, M.V. De Weert, H. Grohganz, J. Rantanen, Fuzzy logic-based expert system for evaluating cake quality of freeze-dried formulations, J. Pharm. Sci. 102 (2013) 4364–4374.
[28] A. Ganguly, S.L. Nail, A. Alexeenko, Experimental determination of the key heat transfer mechanisms in pharmaceutical freeze-drying, J. Pharm. Sci. 102 (2013) 1610–1625.
[29] S. Rambhatla, M. Pikal, Heat and mass transfer scale-up issues during freeze-drying, I: Atypical radiation and the edge vial effect, AAPS PharmSciTech 4 (2003) 22–31.
[30] X. Tang, M.J. Pikal, Design of freeze-drying processes for pharmaceuticals: practical advice, Pharm. Res. 21 (2004) 191–200.
[31] W.Y. Kuu, M.J. Doty, C.L. Rebbeck, W.S. Hurst, Y.K. Cho, Gap-freezing approach for shortening the lyophilization cycle time of pharmaceutical formulations? demonstration of the concept, J. Pharm. Sci. 102 (2013) 2572–2588.
[32] A.K. Konstantinidis, W. Kuu, L. Otten, S.L. Nail, R.R. Sever, Controlled nucleation in freeze-drying: effects on pore size in the dried product layer, mass transfer resistance, and primary drying rate, J. Pharm. Sci. 100 (2011) 3453–3470.
[33] K. Nakagawa, A. Hottot, S. Vessot, J. Andrieu, Modeling of freezing step during freeze-drying of drugs in vials, AIChE J. 53 (2007) 1362–1372.
[34] S. Passot, M. Galan, G.J. Morris, F. Fonseca, I.C. Tréléa, M. Marin, Effect of controlled ice nucleation on primary drying stage and protein recovery in vials cooled in a modified freeze-dryer, J. Biomech. Eng. 131 (2009) 074511-1–074511-5.
[35] S. Hibler, C. Wagner, H. Gieseler, Comparison of product drying performance in molded and serum tubing vials using gentamicin sulfate as a model system, Pharm. Dev. Technol. 17 (2012) 541–551.
[36] S. Hibler, C. Wagner, H. Gieseler, Vial freeze-drying, Part 1: New insights into heat transfer characteristics of tubing and molded vials, J. Pharm. Sci. 101 (2012) 1189–1201.
[37] D. Fissore, A.A. Barresi, Scale-up and process transfer of freeze-drying recipes, Dry. Technol. 29 (2011) 1673–1684.
[38] A. Kauppinen, M. Toiviainen, J. Aaltonen, O. Korhonen, K. Järvinen, M. Juuti, R. Pellinen, J. Ketolainen, Microscale freeze-drying with Raman spectroscopy as a tool for process development, Anal. Chem. 85 (2013) 2109–2116.

Please cite this article in press as: B.-H. Peters et al., Structural attributes of model protein formulations prepared by rapid freeze-drying cycles in a micro-scale heating stage, Eur. J. Pharm. Biopharm. (2014), http://dx.doi.org/10.1016/j.ejpb.2014.02.016